

## Strong coupling of a single ion to an optical cavity

Article (Accepted Version)

Takahashi, Hiroki, Kassa, Ezra, Christoforou, Costas and Keller, Matthias (2020) Strong coupling of a single ion to an optical cavity. *Physical Review Letters (PRL)*, 124 (1). a013602. ISSN 0031-9007

This version is available from Sussex Research Online: <http://sro.sussex.ac.uk/id/eprint/88392/>

This document is made available in accordance with publisher policies and may differ from the published version or from the version of record. If you wish to cite this item you are advised to consult the publisher's version. Please see the URL above for details on accessing the published version.

### **Copyright and reuse:**

Sussex Research Online is a digital repository of the research output of the University.

Copyright and all moral rights to the version of the paper presented here belong to the individual author(s) and/or other copyright owners. To the extent reasonable and practicable, the material made available in SRO has been checked for eligibility before being made available.

Copies of full text items generally can be reproduced, displayed or performed and given to third parties in any format or medium for personal research or study, educational, or not-for-profit purposes without prior permission or charge, provided that the authors, title and full bibliographic details are credited, a hyperlink and/or URL is given for the original metadata page and the content is not changed in any way.

# Strong coupling of a single ion to an optical cavity

Hiroki Takahashi,\* Ezra Kassa, Costas Christoforou, and Matthias Keller

*Department of Physics and Astronomy, University of Sussex, Brighton, BN1 9QH, United Kingdom*

Strong coupling between an atom and an electromagnetic resonator is an important condition in cavity quantum electrodynamics (CQED). While strong coupling in various physical systems has been achieved so far, it remained elusive for single atomic ions. Here we achieve a coupling strength of  $2\pi \times (12.3 \pm 0.1)$  MHz between a single  $^{40}\text{Ca}^+$  ion and an optical cavity, exceeding both atomic and cavity decay rates which are  $2\pi \times 11.5$  and  $2\pi \times (4.1 \pm 0.1)$  MHz respectively. We use cavity assisted Raman spectroscopy to precisely characterize the ion-cavity coupling strength and observe a spectrum featuring the normal mode splitting in the cavity transmission due to the ion-cavity interaction. Our work paves the way towards new applications of CQED utilizing single trapped ions in the strong coupling regime for quantum optics and quantum technologies.

Coupling between atoms and electromagnetic fields is a ubiquitous physical process that underlies a plenitude of electromagnetic phenomena. In cavity quantum electrodynamics (CQED), this interaction is studied in its simplest form where a single atomic emitter is coupled to well-defined electromagnetic modes of a resonator [1, 2]. In many applications of CQED, the coherent atom-photon interaction rate needs to exceed the decoherence rates of the system. This so-called strong coupling regime has been attained in many physical systems including neutral atoms [3, 4], solid state systems [5–8] and an ensemble of trapped ions [9]. Strongly coupled light-matter systems resulted in remarkable applications such as a one-atom optical switch [10] and a quantum optical circulator [11]. However, despite decade long attempts [9, 12–20] strong coupling has remained elusive for single trapped ions until now.

Due to their outstanding properties such as long coherence times [21] and the ability of high-fidelity quantum control [22], trapped ions are a leading system for optical atomic clocks [23, 24], quantum metrology [25, 26] and quantum computation [27, 28]. The setting of CQED brings about exciting possibilities to connect individual quantum devices by providing efficient quantum interfaces with optical photons [29]. Compared to single ions in free space [30, 31], the entanglement generation efficiency of remote ions based on strongly-coupled ion-cavity systems is enhanced by orders of magnitude [32]. This enables the distributed architecture for large-scale quantum information processing using photonic networks [33]. Here, by coupling a single ion to an optical cavity in the strong coupling regime for the first time, we demonstrate a key milestone for this enabling technology.

In the past, conventional Fabry-Perot cavities with macroscopic mirrors were successfully combined with ion traps [14, 17, 18]. In these experiments, however, the ion-cavity coupling was in the weak coupling regime. Since the emitter-cavity coupling scales as  $\propto 1/\sqrt{V_m}$  where  $V_m$  is the mode volume of the cavity, it is essential to reduce  $V_m$  to achieve strong coupling. The main challenge in ion-cavity systems is to achieve small mode volume without disturbing the trapping field when incorporating dielectric cavity mirrors near the trapping region. Employing laser machined fiber-based Fabry-Perot cavities (FFPCs) has proven to be a viable so-

lution for this purpose and resulted in several successful implementations recently [19, 20, 34]. However none of these experiments achieved a coupling strength which exceeds the atomic and cavity decay rates simultaneously. Based on the ion trap with an integrated FFPC presented in [34] and the technique to precisely position the ion in the cavity field [35], in this work we achieve a coherent ion-cavity coupling of  $g = 2\pi \times (12.3 \pm 0.1)$  MHz greater than both atomic decay rate of the  $P_{1/2}$  state of  $\gamma = 2\pi \times 11.5$  MHz [36] and cavity decay rate of  $\kappa = 2\pi \times (4.1 \pm 0.1)$  MHz [32]. This gives us a cooperativity ( $= g^2/\gamma\kappa$ ) of 3.2, on a par with the highest value achieved for an ion-cavity system [17] but with a considerably higher photon extraction rate.

Our experimental apparatus is an endcap-style Paul trap for  $^{40}\text{Ca}^+$  ions with an integrated FFPC (see Fig. 1(a)). The details of the trap can be found in [32, 34, 35]. The FFPC is coupled to the electronic transition between  $P_{1/2}$  and  $D_{3/2}$  states of at 866 nm (see Fig. 1(b)). The cavity field decay rate  $\kappa$  is measured to be  $2\pi \times (4.1 \pm 0.1)$  MHz [32]. Two radial electrodes (RE3 and RE4) are used to displace the rf potential minimum by applying signals synchronous and in-phase to the main drive [35] (RE1 and RE2 are used for the micro-motion compensation). In this way the ion is translated radially without incurring excess micromotion. Using a trapped ion as a probe for the cavity field [35], we determine that the center of the  $\text{TEM}_{00}$  cavity mode is located at  $(3.4 \pm 0.1, 6.4 \pm 0.3) \mu\text{m}$  in the  $x$  and  $y$  directions respectively from the ion's original position when no rf signals are applied to RE3 and RE4. The ion is Doppler cooled on the  $S_{1/2} - P_{3/2}$  transition with a laser at 393 nm to circumvent inefficient cooling on the the  $S_{1/2} - P_{1/2}$  transition caused by the strong Purcell effect when the cavity is near resonant on the  $P_{1/2} - D_{3/2}$  transition [34]. Lasers at 850 nm and 854 nm repump the ion from the meta-stable  $D$  states into the  $S_{1/2}$  state for continuous cooling. Three laser beams at 866 nm (beams I, II and III) with individual polarization controls are used for optical pumping and probing of the ion. Two of them (beam II and III) are injected into the input SM fiber to drive the FFPC. A laser beam at 897 nm is also sent into the FFPC through the SM fiber with its transmission used to stabilize the length of the FFPC.

Having moved the ion to the radial center of the FFPC, we

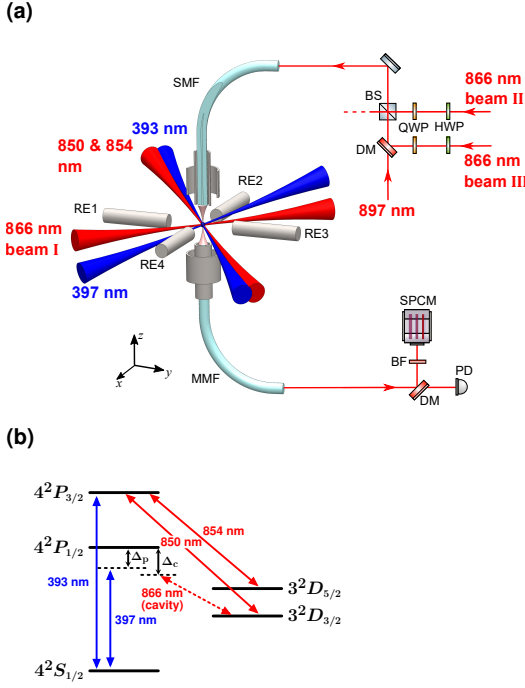


FIG. 1. (a) A schematic of the experimental setup. BF: bandpass filter, BS: beam splitter, DM: dichroic mirror, HWP: half wave plate, MMF: multimode fiber, PD: photodiode, QWP: quarter wave plate, RE: radial electrode, SMF: single-mode fiber, SPCM: single photon counting module. (b) Energy levels of  $^{40}\text{Ca}^+$  ion with driving lasers and the cavity on the relevant transitions.

now characterize  $g_0$  with the optimized overlap at the anti-node of the cavity. The ion-cavity coupling is quantified by analyzing the single-photon emission spectra of the ion-cavity system. Fig. 2(a) shows the pulse sequences of the lasers for this measurement. In combination with the cavity locked close to the  $P_{1/2} - D_{3/2}$  transition with a detuning  $\Delta_c$ , a short pulse of the 397 nm laser with a detuning  $\Delta_p$  results in a single photon in the cavity via a vacuum-stimulated Raman transition from the  $S_{1/2}$  to  $D_{3/2}$  state [14]. Normally the Raman resonance condition dictates  $\Delta_p = \Delta_c$ . However, due to the dressing of the ion's states by the cavity photons, the resonance frequency of the  $P_{1/2} - D_{3/2}$  transition and therefore the Raman resonance are shifted [37]. Fig. 2(b) shows a spectrum of single photon emission as a function of  $\Delta_c$  while  $\Delta_p$  is fixed at -10 MHz. It can be clearly seen that the peak frequency of the spectrum is shifted by an amount  $\delta$  from the expected  $\Delta_p = \Delta_c$  condition. We repeat this Raman spectroscopy for different  $\Delta_p$  as shown in Fig. 2(c) to measure the dependence of  $\delta$  on  $\Delta_p$ . The frequency shift  $\delta$  exhibits a dispersion-like profile whose amplitude and gradient depend on the magnitude of  $g_0$ . Because  $\delta$  also depends on the Rabi frequency  $\Omega_{397}$  of the 397 nm laser through its own ac Stark shift, we independently measure  $\Omega_{397}$  to be  $2\pi \times (11.9 \pm 0.4)$  MHz by the electron shelving method employed in [34]. Given  $\Omega_{397}$  and other known experimental pa-

rameters such as the beam detunings, beam polarizations and the magnetic field, the single-photon emission spectrum and hence  $\delta$  can be precisely simulated by solving time-dependent master equations with  $g_0$  as the only free parameter (see the inset of Fig. 2(d) and [32]). Utilizing the dependence of  $\delta$  on  $g_0$  and fitting this numerical model to the experimental data as shown in Fig. 2(d), we obtain the coherent ion-cavity coupling  $g_0 = 2\pi \times (15.1 \pm 0.1)$  MHz [32].

A small magnetic field ( $= 0.9$  gauss) is applied to align the quantization axis to the cavity axis such that the cavity supports two distinct polarizations  $\sigma_+$  and  $\sigma_-$ . As shown in Fig. 3(a), the ion is simultaneously coupled to these two polarization modes on the transitions connecting the Zeeman sublevels in the  $P_{1/2}$  and  $D_{3/2}$  state manifolds. This configuration effectively realizes a closed three-level lambda system interconnected via a bimodal cavity. When a two-level atom is coupled to a single optical mode, there are two dressed states  $(|g, 1\rangle + |e, 0\rangle)/\sqrt{2}$  and  $(|g, 1\rangle - |e, 0\rangle)/\sqrt{2}$  with an energy gap  $2g$  ( $\hbar = 1$ ) in the subspace for the first excitation from the ground state ( $= |g, 0\rangle$ ) (see Fig. 3(b)). Here  $g$  and  $e$  denote the ground and excited states of the atom respectively, and 0 and 1 denote the intracavity photon number. As a result, a coherent oscillation between  $|g, 1\rangle$  and  $|e, 0\rangle$  occurs at the vacuum Rabi frequency of  $2g$ . Similarly, for the bimodal system with three atomic levels, the subspace for the first excitation includes three originally degenerate states  $|a, 1, 0\rangle$ ,  $|b, 0, 1\rangle$  and  $|c, 0, 0\rangle$ . Here the notation indicates a product of the atomic state and the photon number states of the two cavity modes (see Fig. 3(c) for the labeling of the atomic levels). Due to the atom-cavity coupling, the system now has the following three dressed states:

$$|u_+\rangle = \frac{g_1|a, 1, 0\rangle + g_2|b, 0, 1\rangle + \lambda|c, 0, 0\rangle}{\sqrt{2}\lambda}, \quad (1)$$

$$|u_0\rangle = \frac{g_2|a, 1, 0\rangle - g_1|b, 0, 1\rangle}{\lambda}, \quad (2)$$

$$|u_-\rangle = \frac{g_1|a, 1, 0\rangle + g_2|b, 0, 1\rangle - \lambda|c, 0, 0\rangle}{\sqrt{2}\lambda}, \quad (3)$$

where  $\lambda = \sqrt{g_1^2 + g_2^2}$ . Note that  $|u_0\rangle$  is a dark state which is decoupled from the excited atomic upper state  $|c\rangle$ . The emergence of this state is very similar to the effect of electromagnetically induced transparency (EIT) [38]. The difference here is that the quantized cavity fields, instead of classical lasers, interconnect the three atomic levels. On the other hand, a *bright state* can also be constructed as  $|v\rangle = (g_1|a, 1, 0\rangle + g_2|b, 0, 1\rangle)/\lambda$  in which the excitation amplitudes to  $|c, 0, 0\rangle$  from the constituent states interfere constructively.  $|u_+\rangle$  and  $|u_-\rangle$  can be expressed as

$$|u_{\pm}\rangle = \frac{|v\rangle \pm |c, 0, 0\rangle}{\sqrt{2}}, \quad (4)$$

with an energy gap of  $2\lambda$  (Fig. 3(c)). Consequently, in the same way as between  $|g, 1\rangle$  and  $|e, 0\rangle$  in the two-level case, the coherent oscillation occurs between  $|v\rangle$  and  $|c, 0, 0\rangle$  at a

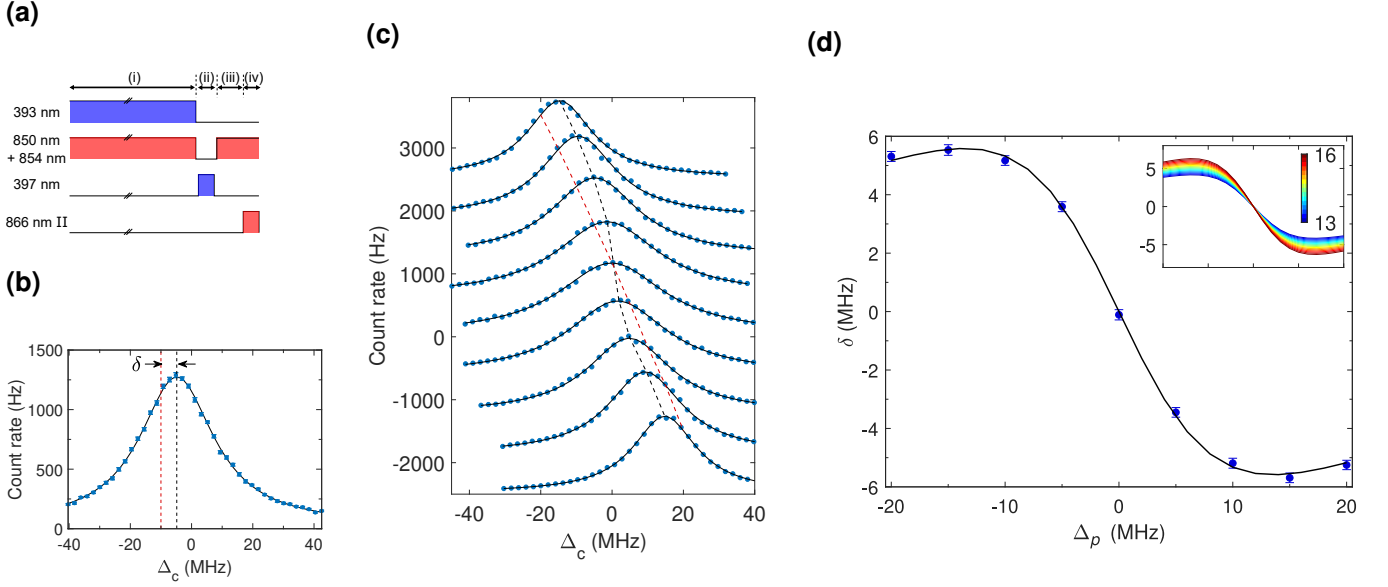


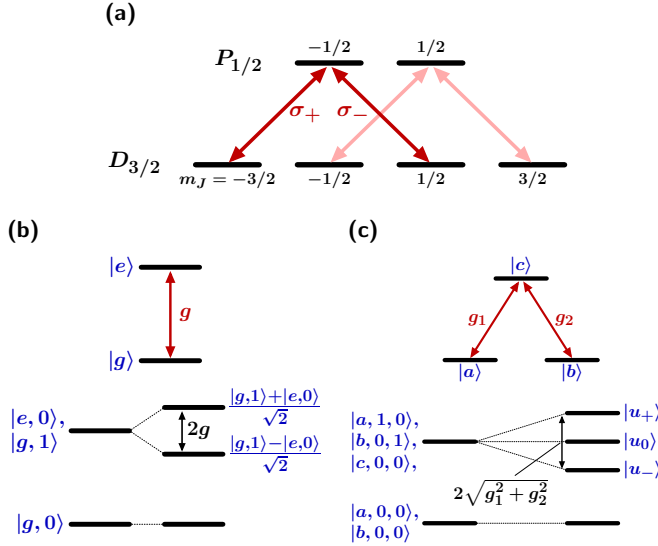
FIG. 2. **(a)** The pulse sequences for the single-photon generation: (i) Doppler cooling for  $6 \mu\text{s}$ . (ii) 300 ns-long pulse of the 397 nm laser to generate a single photon in the cavity. (iii) Recycling the ion's population back to the  $S_{1/2}$  state for 500 ns. (iv) A pulse of the 866 nm laser is injected to the cavity. The 866 nm laser is frequency-locked to the exact resonance to the  $P_{1/2} - D_{3/2}$  transition. Therefore its transmission peak provides an absolute frequency reference for  $\Delta_c$ . **(b)** Single-photon emission spectrum as a function of  $\Delta_c$  with  $\Delta_p$  at -10 MHz. The solid line is a Lorentzian fit. The vertical dashed lines indicate the center frequency of the peak (black) and the frequency expected from the condition  $\Delta_p = \Delta_c$  (red). The same applies to the dashed lines in (c). **(c)** Single-photon emission spectra with different  $\Delta_p$ . From the top to the bottom traces,  $\Delta_p$  varies from -20 to +20 MHz with an interval of 5 MHz. **(d)** The shift of the Raman resonance  $\delta$  as a function of  $\Delta_p$  from the data set in (c). The error bars are the statistical mean standard errors. The solid line is a fit by the numerical simulation. The inset figure shows superimposed traces of  $\delta$  from numerical simulations with different  $g_0/(2\pi)$ . The variation of  $g_0/(2\pi)$  from 13 to 16 MHz is represented by the line colors.

frequency of  $2\lambda$ . This oscillation corresponds to the characteristic emission (and absorption) of a single photon into (and from) the two optical modes simultaneously in a superposition. Hence the vacuum Rabi frequency—the frequency at which a single excitation is exchanged between the atomic and optical degrees of freedom—is given by  $2g = 2\lambda$ .

Applying this picture to the actual energy levels of  $^{40}\text{Ca}^+$  in Fig. 3(a),  $g_1$  and  $g_2$  are derived from  $g_0$  by multiplication with the Clebsh-Gordan coefficients for the  $\sigma_+$  and  $\sigma_-$  transitions, which are  $1/\sqrt{2}$  and  $1/\sqrt{6}$  respectively. With  $g_0 = 2\pi \times (15.1 \pm 0.1) \text{ MHz}$ ,  $g = 2\pi \times (12.3 \pm 0.1) \text{ MHz}$  is obtained. Therefore the coupling of the single ion to the cavity  $g$  exceeds both the atomic decay rate of the  $P_{1/2}$  level  $\gamma$  ( $=2\pi \times 11.5 \text{ MHz}$ ) [36] and the cavity decay rate  $\kappa$  ( $=2\pi \times (4.1 \pm 0.1) \text{ MHz}$ ), placing our system in the strong coupling regime ( $g > \gamma, \kappa$ ).

The characteristic vacuum Rabi splitting in the three-level bimodal system as shown in Fig. 3(c) can be probed by weakly driving the cavity and detecting the transmission. Fig. 4(a) shows the expected spectrum of the transmitted photons when the ideal three-level bimodal system is probed with a near-resonant coherent light. There are three underlying resonant peaks corresponding to the three distinct excitations from the ground state. Fig. 4(b) shows the laser pulse sequences used to probe this in the experiment. Beam I and

II of the 866 nm laser are applied with  $\pi$  and  $\sigma_-$  polarizations respectively in order to optically pump the ion into the  $D_{3/2}$   $m_J = -3/2$  state. Subsequently a pulse of beam III in the  $\sigma_+$  polarization is injected and its transmission through the FFPC is measured. The FFPC is locked to the atomic resonance ( $\Delta_c = 0$ ). The intensity of beam III in the cavity is estimated in terms of the displacement amplitude to the intra-cavity field [32]. Fig. 4(c) shows the resulting spectrum of the transmitted photons as the detuning of beam III from the atomic resonance ( $\equiv \Delta_{866}$ ) is scanned. The spectrum is significantly modified by the ion-cavity coupling (see the inset of Fig. 4c). The data shows good agreement with the numerical simulation shown as the black solid line in Fig. 4(c). Only the vertical scaling and a small horizontal offset ( $\sim 0.47 \text{ MHz}$ ) are adjusted to fit the simulated curve to the measured data. The horizontal offset is likely to have resulted from an error in the calibration of the frequency of the 866 nm laser. The figure also shows the simulated contributions of the excitations to the individual dressed states and contribution from other states. There is a finite probability that the probing laser excites the ion and incoherently distributes its population via spontaneous decays from the  $P_{1/2}$  state. This results in transmission of subsequent photons without interacting with the ion and creates the central peak in a dashed yellow line in the figure. Note that this probability increases as  $g$  increases and hence progressively



fewer photons are required to probe the system, whereas in practice a certain number of photons are required at the detector to ensure a decent signal-to-noise ratio. Despite this noise, the wings of the observed spectrum indicate the deviation from a single-peaked structure and the presence of the dressed states  $|u_{\pm}\rangle$  with an expected separation of  $2g$ .

In conclusion, we have achieved the strong coupling regime for the first time with a single ion, where the vacuum Rabi frequency exceeds both atomic and cavity decoherence rates. Moreover the characteristic energy structure of the dressed-states inherent to our coupled ion-cavity system has been successfully probed by spectroscopic means. The key milestones that have led to this work are the overcoming of practical limitations that have limited the successful integration of an ion traps with a miniature cavity for decades and the ability to precisely control the ion's position in the cavity mode. Strong coupling between a single ion and an optical cavity facilitates novel opportunities to combine the unparalleled capabilities of trapped ions with quantum photonics. It enables applications such as highly efficient single photon sources and high fidelity ion-photon quantum interfaces, key components in quantum networks and quantum computing. Without further optimisation, a numerical study shows that a heralded entanglement efficiency of 1.7% at a rate of 8.5 kHz between two remote ions can be achieved, a factor of  $\sim 1900$  improvement over previous work [30]. Moreover our FFPC can be readily mod-

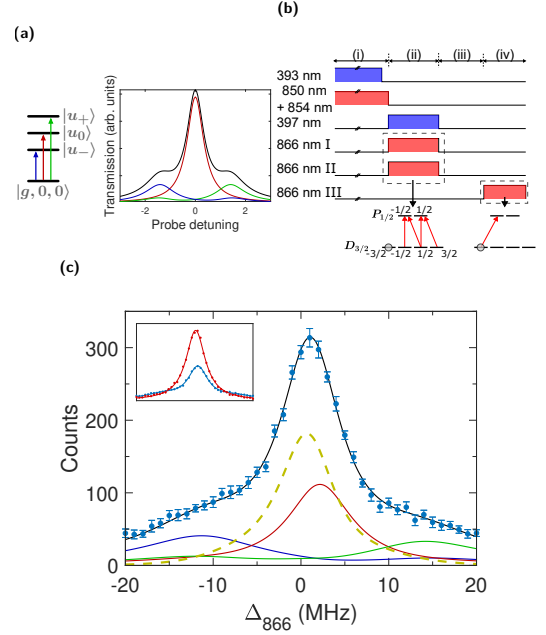


FIG. 4. (a) A model calculation for the ideal three-level system. The solid line shows the expected spectrum of transmitted photons as a function of the probe detuning. Here  $g_1 = g_2 = g$  and the probe frequency is normalized by  $g$ . The underlying contributions of the individual dressed states in the level diagram on the left are shown in the same colors as the corresponding excitations in the level diagram on the left. (b) Laser pulse sequences: (i) 5  $\mu\text{s}$ -long Doppler cooling. The duration of the repumping beams is longer than that of the 393 nm beam in order to prepare the ion in the  $S_{1/2}$  state. (ii) Optical pumping for 3  $\mu\text{s}$ . (iii) An interval is placed in order to wait for the intensities of the optical pumping lasers to sufficiently diminish. (iv) Probing with beam III. (c) The counts of the transmitted photons of beam III as a function of its detuning. The background counts ( $\sim 90$ ) from stray light are subtracted. The solid black line is the result of numerical calculation (see the main text). The underlying contributions are also shown with the same color scheme as in (a). In addition the contribution from non-dressed states is shown in the yellow dashed line. The inset also shows a spectrum taken without the ion (red) superposed with the spectrum with the ion (blue).

ified to further enhance the single-photon generation efficiency by simply increasing the external coupling of one of the cavity mirrors or optimizing the mirror geometry [32, 39].

## ACKNOWLEDGMENTS

We gratefully acknowledge support from EPSRC through the UK Quantum Technology Hub: NQIT - Networked Quantum Information Technologies (EP/M013243/1 and EP/J003670/1).

---

\* email: takahashi@qc.rcast.u-tokyo.ac.jp

Present address: Research Center for Advanced Science and Technology, the University of Tokyo, Meguro-ku, Tokyo 153-8904, Japan

- [1] H. J. Kimble, *Physica Scripta* **1998**, 127 (1998).
- [2] S. Girvin, M. Devoret, and R. Schoelkopf, *Physica Scripta* **2009**, 014012 (2009).
- [3] A. Boca, R. Miller, K. Birnbaum, A. Boozer, J. McKeever, and H. Kimble, *Phys. Rev. Lett.* **93**, 233603 (2004).
- [4] P. Maunz, T. Puppe, I. Schuster, N. Syassen, P. W. Pinkse, and G. Rempe, *Phys. Rev. Lett.* **94**, 033002 (2005).
- [5] J. P. Reithmaier, G. Sek, A. Löffler, C. Hofmann, S. Kuhn, S. Reitzenstein, L. V. Keldysh, V. D. Kulakovskii, T. L. Reinecke, and A. Forchel, *Nature* **432**, 197 (2004).
- [6] T. Yoshie, A. Scherer, J. Hendrickson, G. Khitrova, H. Gibbs, G. Rupper, C. Ell, O. Shchekin, and D. Deppe, *Nature* **432**, 200 (2004).
- [7] A. Wallraff, D. I. Schuster, A. Blais, L. Frunzio, J. Majer, S. Kumar, S. M. Girvin, and R. J. Schoelkopf, *Nature* **431**, 162 (2004).
- [8] I. Chiorescu, P. Bertet, K. Semba, Y. Nakamura, C. Harmans, and J. Mooij, *Nature* **431**, 159 (2004).
- [9] P. F. Herskind, A. Dantan, J. P. Marler, M. Albert, and M. Drewsen, *Nature Physics* **5**, 494 (2009).
- [10] I. Shomroni, S. Rosenblum, Y. Lovsky, O. Bechler, G. Guelandelman, and B. Dayan, *Science* **345**, 903 (2014).
- [11] M. Scheucher, A. Hilico, E. Will, J. Volz, and A. Rauschenbeutel, *Science* **354**, 1577 (2016).
- [12] G. R. Guthöhrlein, M. Keller, K. Hayasaka, W. Lange, and H. Walther, *Nature* **414**, 49 (2001).
- [13] A. B. Mundt, A. Kreuter, C. Becher, D. Leibfried, J. Eschner, F. Schmidt-Kaler, and R. Blatt, *Phys. Rev. Lett.* **89**, 103001 (2002).
- [14] M. Keller, B. Lange, K. Hayasaka, W. Lange, and H. Walther, *Nature* **431**, 1075 (2004).
- [15] D. R. Leibbrandt, J. Labaziewicz, V. Vuletić, and I. L. Chuang, *Phys. Rev. Lett.* **103**, 103001 (2009).
- [16] J. D. Sterk, L. Luo, T. A. Manning, P. Maunz, and C. Monroe, *Phys. Rev. A* **85**, 062308 (2012).
- [17] A. Stute, B. Casabone, P. Schindler, T. Monz, P. Schmidt, B. Brandstätter, T. Northup, and R. Blatt, *Nature* **485**, 482 (2012).
- [18] A. Stute, B. Casabone, B. Brandstätter, K. Friebe, T. Northup, and R. Blatt, *Nature Photonics* **7**, 219 (2013).
- [19] M. Steiner, H. M. Meyer, C. Deutsch, J. Reichel, and M. Köhl, *Phys. Rev. Lett.* **110**, 043003 (2013).
- [20] T. G. Ballance, H. M. Meyer, P. Kobel, K. Ott, J. Reichel, and M. Köhl, *Phys. Rev. A* **95**, 033812 (2017).
- [21] T. P. Harty, D. T. C. Allcock, C. J. Ballance, L. Guidoni, H. A. Janacek, N. M. Linke, D. N. Stacey, and D. M. Lucas, *Phys. Rev. Lett.* **113**, 220501 (2014).
- [22] C. J. Ballance, T. P. Harty, N. M. Linke, M. A. Sepiol, and D. M. Lucas, *Phys. Rev. Lett.* **117**, 060504 (2016).
- [23] C. W. Chou, D. B. Hume, J. C. J. Koelemeij, D. J. Wineland, and T. Rosenband, *Physical Review Letters* **104**, 070802 (2010).
- [24] N. Huntemann, C. Sanner, B. Lipphardt, C. Tamm, and E. Peik, *Phys. Rev. Lett.* **116**, 063001 (2016).
- [25] S. Kotler, N. Akerman, Y. Glickman, A. Keselman, and R. Ozeri, *Nature* **473**, 61 (2011).
- [26] I. Baumgart, J.-M. Cai, A. Retzker, M. Plenio, and C. Wunderlich, *Phys. Rev. Lett.* **116**, 240801 (2016).
- [27] S. Debnath, N. M. Linke, C. Figgatt, K. A. Landsman, K. Wright, and C. Monroe, *Nature* **536**, 63 (2016).
- [28] T. Monz, D. Nigg, E. A. Martinez, M. F. Brandl, P. Schindler, R. Rines, S. X. Wang, I. L. Chuang, and R. Blatt, *Science* **351**, 1068 (2016).
- [29] H. J. Kimble, *Nature* **453**, 1023 (2008).
- [30] D. Hucul, I. Inlek, G. Vittorini, C. Crocker, S. Debnath, S. Clark, and C. Monroe, *Nature Physics* **11**, 37 (2015).
- [31] C. Crocker, M. Lichtman, K. Sosnova, A. Carter, S. Scarano, and C. Monroe, *arXiv:1812.01749* (2018).
- [32] See the Supplemental Material.
- [33] C. Monroe, R. Raussendorf, A. Ruthven, K. R. Brown, P. Maunz, L.-M. Duan, and J. Kim, *Phys. Rev. A* **89**, 022317 (2014).
- [34] H. Takahashi, E. Kassa, C. Christoforou, and M. Keller, *Phys. Rev. A* **96**, 023824 (2017).
- [35] E. Kassa, H. Takahashi, C. Christoforou, and M. Keller, *Journal of Modern Optics* **65**, 520 (2018).
- [36] M. Hettrich, T. Ruster, H. Kaufmann, C. F. Roos, C. T. Schmiegelow, F. Schmidt-Kaler, and U. G. Poschinger, *Phys. Rev. Lett.* **115**, 143003 (2015).
- [37] M. Albert, J. Marler, P. F. Herskind, A. Dantan, and M. Drewsen, *Phys. Rev. A* **85**, 023818 (2012).
- [38] M. Fleischhauer, A. Imamoglu, and J. P. Marangos, *Rev. Mod. Phys.* **77**, 633 (2005).
- [39] K. Ott, S. Garcia, R. Kohlhaas, K. Schüppert, P. Rosenbusch, R. Long, and J. Reichel, *Optics Express* **24**, 9839 (2016).